DOI: https://doi.org/10.24425/amm.2025.154461

MIN-JI KIM[©]^{1,2}, MIN-JEONG LEE[©]^{1,2}, HYUN-JU KIM[©]¹, JU-YONG KIM[©]³, JUNG-WOO LEE[©]^{2*}, JUNG-YEUL YUN[©]^{1*}

FABRICATING METAL POWDER FILTERS WITH MATERIAL EXTRUSION ADDITIVE MANUFACTURING

Metal powder filters are key components in semiconductor manufacturing equipment that play a critical role in preventing the ingress of impurities and fine particles that may be contained in process gases. With the increasingly advanced development of the semiconductor industry, metal powder filters also require more precise and advanced performance. Therefore, in this study, a filter with a honeycomb structure morphology with crossed top and bottom was fabricated by a material extrusion additive manufacturing (MEAM) process. To achieve this, the prepared pellets were subjected to the MEAM, allowing the creation of filters with complex shapes featuring crossed top and bottom structures. After polishing the surface of the specimen, solvent debinding and thermal debinding were performed to remove the binder. Solvent debinding was performed in n-Heptane for 24 hours, while thermal debinding was performed in an Ar atmosphere at a maximum temperature of 800°C. The debinded specimens were sintered under a high vacuum atmosphere at temperatures of 850°C, 950°C, and 1050°C, respectively. The prepared metal powder filters were examined for filter morphology and microstructure using optical microscopy, and pore properties such as porosity and air permeability were evaluated.

Keywords: Metal Powder Filters; Sintering; Porosity; Air Permeability; Material Extrusion Additive Manufacturing (MEAM)

1. Introduction

Filters made from porous materials are utilized across various industries, including chemicals, biotechnology, automotive, energy, environment, and semiconductors [1-6]. The advancement and sophistication of the semiconductor industry have led to increased demands for precision in manufacturing processes. In semiconductor manufacturing, maintaining an ultra-clean environment is essential for achieving fine patterns and structures, making the purity and quality of the gases used closely related to the performance of the produced semiconductors. Among these, filters used in the semiconductor industry are critical components that prevent impurities from entering during the gas flow from gas supply facilities through gas distributors to semiconductor production equipment, thereby maintaining process purity, ensuring process stability, protecting equipment, and enhancing product reliability [7-8].

Recently, as the semiconductor process industry has developed, the performance criteria for gas filters have also risen. For example, in nanoscale processes, filters capable of removing ultra-fine particles are required, necessitating filters with precise

pore structures and high air permeability. As a result, traditional simple disc-type or cylindrical tube filters have become inadequate, requiring more complex and precise filter designs. Existing conventional methods face limitations in implementing complex-shaped filters, leading to an increasing focus on filter manufacturing using 3D printing technology [9-11].

Metal-based additive manufacturing (AM) processes can be categorized according to the type of energy source employed: beam-based processes (e.g., Powder Bed Fusion (PBF) and Directed Energy Deposition (DED)) and beamless processes that do not utilize high-energy beams.

PBF and DED selectively melt metal powders using highpower lasers or electron beams, making them well suited for fabricating dense and high-strength metal components. However, these processes often involve local high-temperature exposure, which can induce thermal and residual stresses, require expensive equipment, and entail complex process control.

As an alternative to overcome these limitations, this study adopts the Material Extrusion Additive Manufacturing (MEAM) process. MEAM is a beamless technique in which materials are extruded by thermal softening, without the use of high-energy

^{*} Corresponding authors: yjy1706@kims.re.kr; jungwoolee@pusan.ac.kr



NANOMATERIALS RESEARCH CENTER, KOREA INSTITUTE OF MATERIALS SCIENCE KIMS, CHANGWON 51508, REPUBLIC OF KOREA

² PUSAN NATIONAL UNIVERSITY, DEPARTMENT OF MATERIALS SCIENCE AND ENGINEERING, BUSAN 46241, REPUBLIC OF KOREA

³DP R&D CENTER, REPROTECH, SUWON, 16229, REPUBLIC OF KOREA

beams. This method offers advantages such as simple system configuration, lower equipment costs, and broad material compatibility. In particular, the absence of laser-based systems significantly reduces initial investment requirements. Furthermore, MEAM eliminates the need for mold fabrication, making it highly suitable for prototype production, and provides excellent design flexibility for implementing complex structures [12-18].

In this study is to manufacture filters with more complex structures than conventional cylindrical filters to improve one of the key performance characteristics of filters: air permeability. To this end, a filter with a honeycomb structure morphology featuring crossed top and bottom was fabricated using the MEAM process. Furthermore, the particle sizes of SUS316L powder used in the pellets were varied at 8 μm and 50 μm to control the pore characteristics of the filter.

2. Experimental

A schematic diagram of the process for manufacturing the honeycomb-structured filter with crossed top and bottom is shown in Fig. 1. In this study, two types of pellets made from SUS316L powder were prepared and then manufactured into a metal powder filter using a MEAM process. Initially, two types of pellets were prepared by mixing a binder with SUS316L powders of different sizes (TABLE 1). The SUS316L powder sizes used were 8 μm and 50 μm , and the binder contents for the pellets were mixed at 7.31 wt.% and 13.66 wt.%, respectively. The prepared pellets were used in the MEAM process to manufacture honeycomb-structured filters with 4-channel and 9-channel configurations, where the top and bottom ends were blocked in a crossed manner. The MEAM process was carried out using a nozzle diameter of 0.4 mm. The extrusion temperature and bed temperature were maintained at 175°C and 65°C, respectively.

The extrusion speed was set to 35 mm/sec, and the layer height (interlayer spacing) was controlled at 125 µm. These printing parameters were optimized to ensure consistent extrusion and stable layer stacking throughout the fabrication process. To prevent air flow obstruction and ensure smooth gas movement caused by potential interlayer irregularities during the layering process using the MEAM method, the surface of the specimens was polished. According to their respective shapes, the specimens were named the 4-channel type and 9-channel type. After the polishing process, the specimens underwent solvent debinding and thermal debinding to remove the binder. Solvent debinding was conducted in an n-Heptane solution for 24 hours, followed by thermal debinding in an argon atmosphere at a maximum temperature of 800°C. The debinded specimens were then sintered in a high vacuum atmosphere at temperatures of 850°C, 950°C, and 1050°C for one hour each to assess the effects of sintering temperature on the filters. The sintering temperature should be set higher than the particle neck formation temperature but lower than the melting point. Within this range, the particles can bond sufficiently while maintaining the pore structure. Excessively high sintering temperatures can lead to excessive densification of the particles, resulting in the loss of the pore structure, while excessively low temperatures may result in insufficient particle bonding, degrading the mechanical properties. Therefore, the sintering temperature was set to a value lower than the melting point of SUS316L (approximately 1370°C), while still being high enough to allow for adequate neck formation.

The completed sintered filters were analyzed for pore characteristics using a capillary flow porometer (CEP1200AEL, PMI, USA) to measure air permeability, and optical microscopy (OM, Nikon ECLIPSE MA200, JAPAN) was employed to observe the microstructure. The pore sizes and porosity were measured using the ImageJ program based on the particle size and sintering temperature.

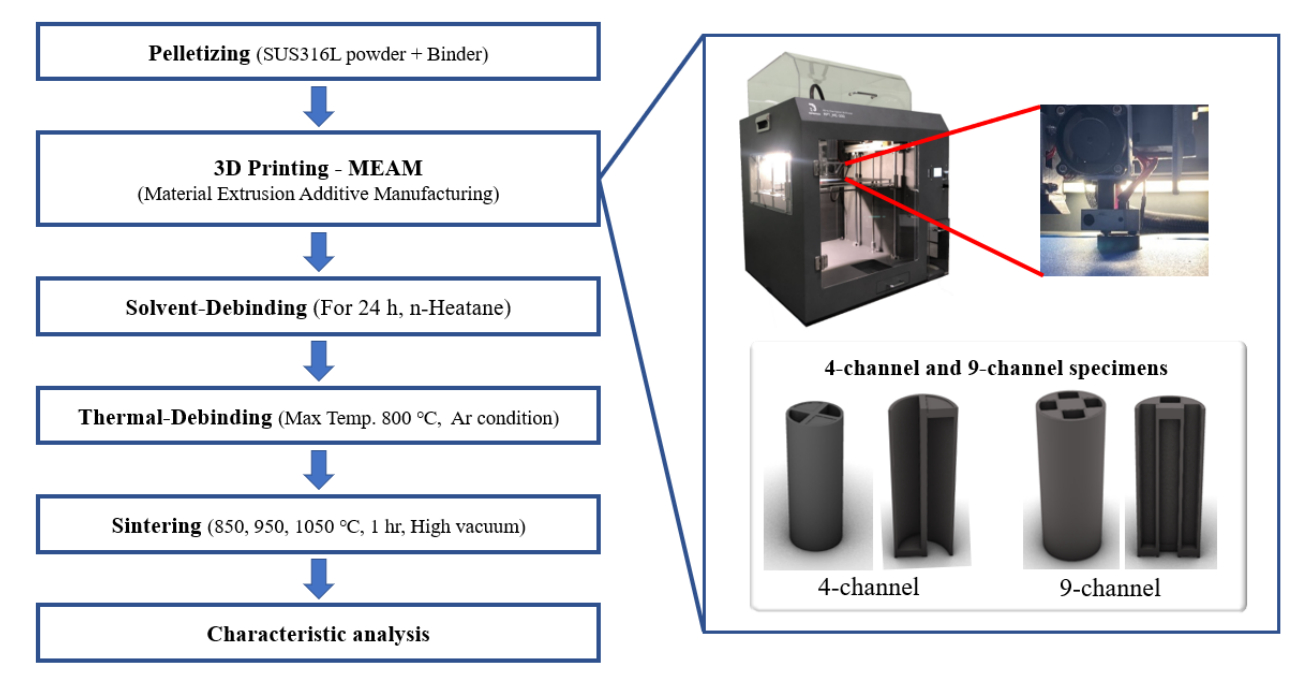


Fig. 1. Schematic of SUS316L Gas filter made with MEAM process

TABLE 1
The percentage of binder content by weight based on the powder particle size

Filament	Powder (wt.%)	Binder (wt.%)
8 μm	92.69	7.31
50 μm	86.34	13.66

3. Results and discussion

Fig. 2 shows the changes in surface roughness of the filters manufactured through the MEAM process. In Fig. 2(a) shows the specimen before polishing, Fig.2(b) shows the specimen after polishing, demonstrating a significant improvement in surface smoothness. The graph on the right illustrates the surface roughness (Ra, μ m) before and after polishing. Before polishing, the roughness of each specimen was approximately 20 to 25 μ m, but after polishing, all specimens exhibited a roughness of about 1 μ m. This confirms that the polishing process effectively re-

duced surface roughness, thereby enhancing the surface quality of the specimens.

In addition to visual improvements, the effect of polishing on surface roughness has functional implications for filter performance. During permeability and filtration testing, the presence of irregularities and protrusions on the outer surface – resulting from the layer-by-layer nature of the MEAM process – can disrupt the smooth flow of air from the external environment into the internal channels of the filter. After polishing, the smoother external surface significantly reduces these flow obstructions. As a result, the improved surface finish facilitates more uniform and efficient airflow through the filter. Therefore, polishing contributed not only to surface quality enhancement but also to the overall functional performance of the filter, especially in terms of air permeability. [22]

Fig. 3 shows (a) the microstructural images and (b) the porosity graph according to particle size and sintering temperature. Fig. 3(a) shows the microstructures of specimens made using different particle sizes (8 μ m and 50 μ m) after sintering at 850°C,

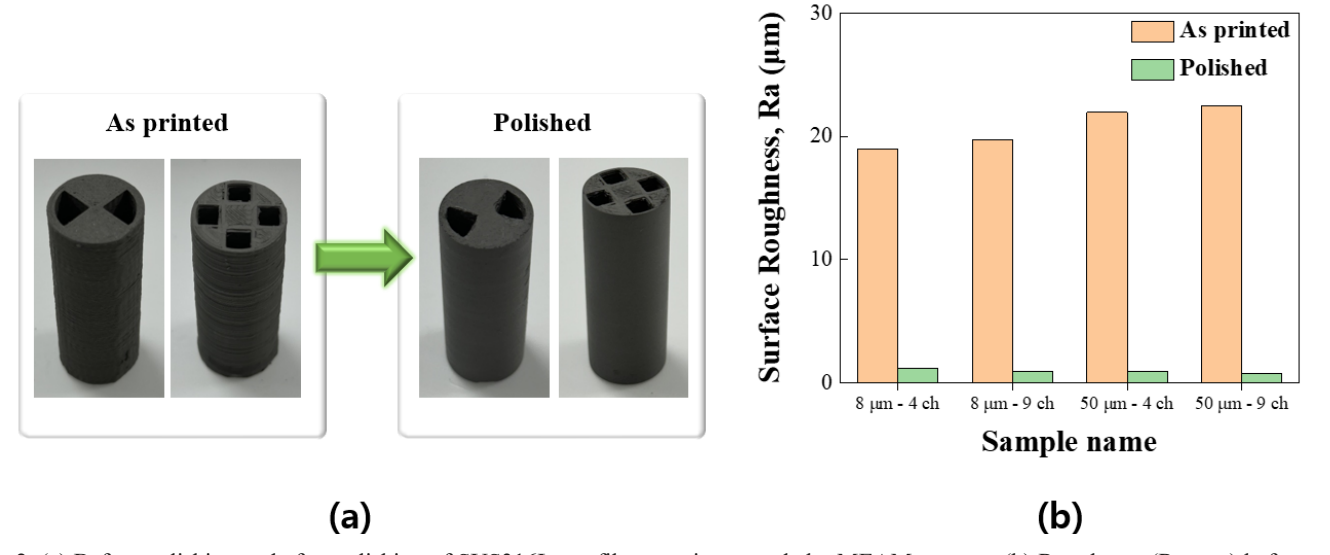


Fig. 2. (a) Before polishing and after polishing of SUS316L gas filter specimen made by MEAM process. (b) Roughness (Ra, μm) before and after polishing

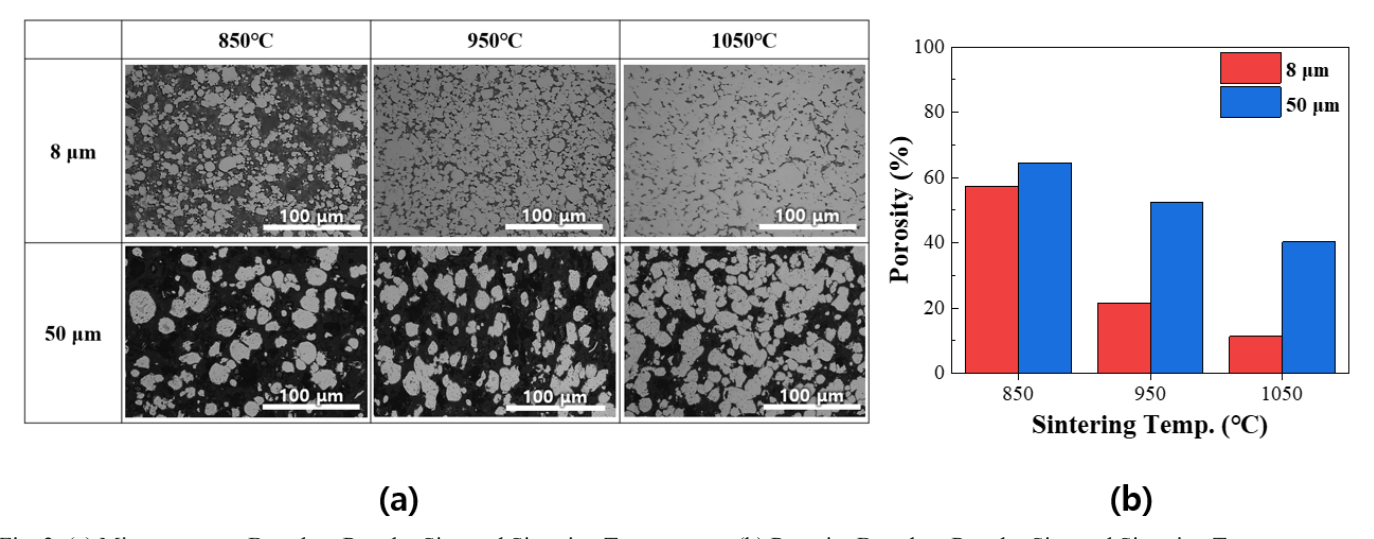


Fig. 3. (a) Microstructure Based on Powder Size and Sintering Temperature, (b) Porosity Based on Powder Size and Sintering Temperature

950°C, and 1050°C. It can be observed that as the sintering temperature increases, the number of pores in the microstructure decreases. Additionally, comparing the specimens made with 8 µm and 50 µm powders at the same sintering temperature reveals that the 50 µm specimens have larger and more abundant pores. Fig. 3(b) shows the change in porosity according to microstructure, indicating that porosity decreases as the sintering temperature rises, and for the same sintering temperature, specimens made with 50 µm powder exhibit higher porosity. This phenomenon can be interpreted as an effect of powder particle size and sintering temperature on microstructure and porosity.

Fig. 4 presents a quantitative analysis of air permeability as influenced by powder size, structural geometry, and sintering temperature. Regarding powder size, specimens fabricated using 50 μ m powder consistently exhibited higher air permeability than those made with 8 μ m powder under identical processing conditions. This can be attributed to the larger interparticle spacing of the 50 μ m powder, which led to less densification during sintering. As a result, the specimens retained higher porosity, which in turn enhanced their air permeability. Larger particles tend to form coarser pore networks, thereby facilitating fluid transport through the porous matrix.

In terms of sintering temperature, a general trend of decreasing air permeability was observed with increasing sintering temperature. At elevated temperatures, intensified diffusion between particles promotes neck growth and grain coalescence, resulting in the closure of micropores. Notably, specimens sintered at 1050°C showed a pronounced reduction in permeability across most conditions, due to the advanced densification and reduced pore interconnectivity.

For the analysis of geometry-dependent air permeability, a comparison was conducted among filters fabricated with 50 μ m powder and sintered at 950°C, including the 4-channel and 9-channel filters produced by 3D printing and a commercially manufactured cylindrical tube filter produced by the conventional press method. The 9-channel filter exhibited superior air permeability relative to the 4-channel design, which is ascribed

to its more complex structure offering a greater number of flow paths. The increased number of channels effectively enhances the permeability by expanding internal flow routes.

Furthermore, under identical testing conditions, both the 4-channel and 9-channel filters fabricated via 3D printing exhibited higher air permeability than the pressed tube-type filter. This can be explained by the limited design flexibility of the press method, which typically yields simple geometries. In contrast, the MEAM (Material Extrusion Additive Manufacturing) technique enables the realization of more complex and open internal architectures that are more favorable for gas flow. Whereas tube-type filters allow only unidirectional flow within a cylindrical cavity, the honeycomb-structured channel filters produced in this study support multidirectional flow, increasing the effective filtration area and simultaneously reducing pressure drop.

In conclusion, Fig. 4 demonstrates the significant effects of particle size, sintering temperature, and filter geometry on air permeability. The results provide experimental validation that complex structural designs enabled by additive manufacturing can achieve enhanced performance compared to conventional commercial filters. These findings suggest that the integration of geometric optimization with additive manufacturing technologies will be a key strategy for the next generation of high-performance metal filter design.

The influence of pore structure on filtration behavior can also be theoretically described using Darcy's law, which relates fluid flow through a porous medium to its permeability:

$$Q = (k A \Delta P) / (\mu L)$$

where Q is the volumetric flow rate, k is the permeability of the porous medium, A is the cross-sectional area, ΔP is the pressure difference across the filter, μ is the fluid viscosity, and L is the filter thickness. According to this model, the permeability (k) – which depends on the pore structure – directly affects the flow rate and, indirectly, the filter's capacity to retain particles. While filtration efficiency was not directly measured in this study, the pore characteristics analyzed herein (size, distribu-

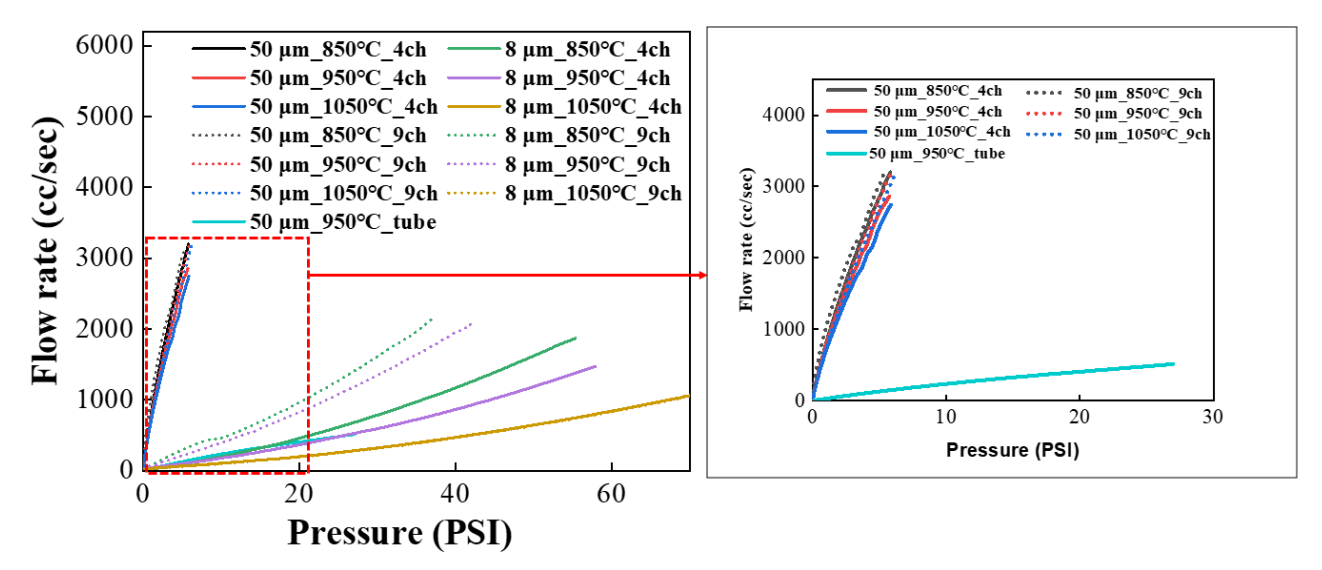


Fig. 4. Porosity Characteristics Based on Sintering Temperature and Shape

tion, and connectivity) are indicative of the filter's potential performance in particle capture applications [19-21].

In this study, the evaluation primarily focused on performance metrics such as air permeability. However, to enable practical implementation in high-purity applications such as semiconductor manufacturing, further investigations are required. These should include quantitative assessments of mechanical stability, including compressive and flexural strength, which are planned for future work.

4. Conclusions

In this study, metal powder filters with 4-channel type and 9-channel type configurations, featuring crossed top and bottom structures, were successfully manufactured using the MEAM process from pellets made with 8 μm and 50 μm powder sizes. The surface roughness of the filters was significantly reduced through the polishing process, confirming the effectiveness of this method in enhancing surface quality. Furthermore, observations of microstructure and porosity changes according to powder size and sintering temperature revealed that as sintering temperature increases, the porosity decreases, while larger powder sizes resulted in more porosity. Notably, specimens made with 50 μm powder exhibited larger pores and higher porosity. The air permeability tests indicated that specimens made with 50 μm powder showed higher air permeability compared to those made with 8 μm powder, particularly at lower sintering temperatures. Additionally, the 9-channel configuration demonstrated greater air permeability than the 4-channel configuration, attributed to improved fluid flow in the 9-channel structure. Overall, these experimental results highlight that powder size, sintering temperature, and channel shape significantly influence the porosity and air permeability of filters, and that utilizing larger particles and complex structures can yield higher air permeability, making these factors critical considerations for future filter design and manufacturing processes.

Acknowledgments

This work is supported by the Ministry of Trade, Industry & Energy (MOTIE) of the Republic of Korea (no. 00431424).

REFERENCES

- [1] S. Rashidi, J. A. Exfahani, A. Rashidi, A review on the applications of porous materials in solar energy systems **176** (2023).
- [2] MaryTheresa M. Pendergast, Eric M.V. Hoek, A review of water treatment membrane nanotechnologies. Energy & Environmental Science 4, 6, 14-15 (2011).
- [3] N.P. Brandon, D.J. Brett, Engineering porous materials for fuel cell applications. Philosophical Transactions of the Royal Society

- A: Mathematical, Physical and Engineering Sciences **364**, 1838 147-159 (2006).
- [4] F. Yalcinkaya, et al., A review on membrane technology and chemical surface modification for the oily wastewater treatment. Materials 13, 2, 5-10 (2020).
- [5] Zhu, Bo, et al., Short review on porous metal membranes Fabrication, commercial products, and applications. **2-19** (2018).
- [6] J. Wang, H. Tang, P. Tan, J. Zhou, Procedia Engineering 27, 737-741 (2012)F.
- [7] Gh. Korotcenkov, B.K. Cho, Porous semiconductors: advanced material for gas sensor applications. Critical Reviews in Solid State and Materials Sciences **35**, 1 1-37 (2010).
- [8] H. Föll, J. Carstensen, S. Frey, Porous and nanoporous semiconductors and emerging applications. Journal of Nanomaterials 2006.1 5-6 (2006).
- [9] Liu, Peisheng, and Guo-Feng Chen, Porous materials: processing and applications. 10-20, 45-60, 80-100, 120-135 (2014).
- [10] C. Osburn, et al., The effects of contamination on semiconductor manufacturing yield. The Journal of Environmental Sciences 31, 2, 45-57 (1988).
- [11] Maire S.A. Heikkinen, N.H. Harley, J. Aerosol. Sci. **31**, 721-738 (2000).
- [12] D.C. Jimenez-Ordonez, et al., Design and 3D printing manufacturing of complex structures for airflow evaluation. Materials and Manufacturing Processes **38**, 8 980-988 (2023).
- [13] Mallikarjuna N. Nadagouda, M. Ginn, V. Rastogi, A review of 3D printing techniques for environmental applications. Current opinion in chemical engineering **28**, 173-178 (2020).
- [14] Zhiyao Ma, et al., Performance analysis and improvement of air filtration and ventilation process in semiconductor clean airconditioning system. Energy and Buildings **228**, 2-4 (2020).
- [15] B.A. Praveena, et al., A comprehensive review of emerging additive manufacturing (3D printing technology): Methods, materials, applications, challenges, trends and future potential. Materials Today: Proceedings **52**, 1309-1313 (2022).
- [16] Goh, Guo Dong, et al., Process-structure-properties in polymer additive manufacturing via material extrusion: A review. Critical Reviews in Solid State and Materials Sciences 45, 2 113-133 (2020).
- [17] Aghnia Ilmiah, Nurhudan, et al., Additive manufacturing of metallic based on extrusion process: A review. Journal of Manufacturing Processes 66, 228-237 (2021).
- [18] M. Vaezi, P. Drescher, H. Seitz, Beamless metal additive manufacturing. Materials **13**, 4, 922 (2020).
- [19] P. Neuman Shlomo, Theoretical derivation of Darcy's law. Acta Mechanica 25, 3 153-170 (1977).
- [20] S. Whitaker, Flow in porous media I: A theoretical derivation of Darcy's law. Transport in Porous Media 1, 3-25 (1986).
- [21] M. King Hubbert, Darcy's law and the field equations of the flow of underground fluids. Transactions of the AIME 207, 01 222-239 (1956).
- [22] N. Mugnier, P. Clérin, J. Sinquin, Industrial experience of polishing filtration performance improvement and interpretation. Light Metals **2001**, 33-39 (2001).